# Theoretical Studies of Ground and Excited Electronic States in a Series of Halide Rhenium(I) Bipyridine Complexes

**Li Yang,[†] Ai-Min Ren,[†] Ji-Kang Feng,\*,[†,‡] Xiao-Juan Liu,[†] Yu-Guang Ma,[§] Ming Zhang,[§] Xiao-Dong Liu,[†,‡] Jia-Cong Shen,[§] and Hong-Xing Zhang[†]**

*State Key Laboratory of Theoretical and Computational Chemistry, Institute of Theoretical Chemistry, Jilin University, Changchun 130023, People's Republic of China, The College of Chemistry, Jilin University, Changchun 130023, People's Republic of China, and Key Lab for Supramolecular Structure and Materials of Ministry of Education, Jilin University, Changchun 130023, People's Republic of China*

*Received: June 23, 2003; In Final Form: June 3, 2004*

Density functional theory (DFT) is applied to analyze ground- and excited-state properties of the Re(I) halide bipyridine complex $ReCl(CO)_3$(bpy) (**1**) and the related complexes $ReCl(CO)_3$(5,5′-dibromo-bpy) (**2**), ReCl-$(CO)_3$(4,4′-dimethyl-bpy) (**3**), and $ReCl(CO)_3$(4,4′-dimethylformyl-bpy) (**4**) (where bpy = 2,2′bipyridine). The electronic properties of the neutral molecules, in addition to the positive and negative ions, are studied using the B3LYP functional. Excited singlet and triplet states are examined using time-dependent DFT (TDDFT). The low-lying excited-state geometries are optimized at the ab initio configuration interaction singlets (CIS) level. As shown, the occupied orbitals involved in the transitions have a significant mixture of the metal Re and the group Cl, by the amount of metal 5d character which varies from 30 to 65%. The lowest unoccupied molecular orbital (LUMO) is a $\pi^*$ orbital of the ligand bpy for the series of molecules. The TDDFT result indicates that the absorption maxima are at relatively high energy and are mainly assigned to bpy-based $\pi\pi^*$ transitions with somewhat metal-to-ligand charge transfer (MLCT) [d(Re) $\rightarrow \pi^*$(bpy)] and ligand-to-ligand charge transfer (LLCT) [p(Cl) $\rightarrow \pi^*$(bpy)] except for complex **3**, in which this band is mainly assigned to mixed MLCT/LLCT, and overlaps bpy $\pi\pi^*$ character. All the low-lying transitions are categorized as mixed MLCT/LLCT. The absorption bands are blue shifted when substituted by an electron-releasing group ($-CH_3$), and they are red shifted when substituted by an electron-withdrawing group ($-Br$ or $-COOCH_3$). The luminescence of all complexes is assigned as a triplet metal/chlorine to bpy charge transfer (MLCT/LLCT).

## Introduction

There has been considerable recent interest in the optical properties of complexes and polymers (or oligomers),[1−4] and particularly the luminescent properties of polypyridine complexes containing $d^6$ metals such as rhenium(I), ruthenium(II), and osmium(II) have been widely investigated in experiments, which shows immense applied prospect.[5−8] Metal-based dyes have proven to perform surprisingly well, and against all odds, some dye molecules were found to be very stable under operating conditions.[9] Their peculiar molecular properties, and the possibilities of related technological applications, are directly related to (a) the energetic spectrum of the molecules that determines the optical absorption and emission characteristics and (b) the molecules electronic structure of the ground as well as of the lowest excited states. The experimental appeal of these molecules lies in the adjustability of their electronic properties through change in the attached ligands and in their easily measured spectroscopic characteristics.[10] As far as we know, very little theoretical work is available on this topic despite the potential interest of an advanced quantum chemical approach

for a better understanding of key issues, such as the nature of both the ground and the excited states involved in the absorption and/or photoemission and its tuning by different substituents.[11−13]

The main difficulties against a reliable computational approach are related to the size of such systems and to the presence of strong electron correlation effects. Both properties are difficult to treat in the framework of the quantum mechanical methods rooted in the Hartree−Fock (HF) theory. As a matter of fact, the post-HF methods needed to obtain reliable excited-state properties have scaling properties with the number of electrons ($N^6$ or worse) that prevent their application to large systems. Recently, investigations have been carried out at the approximate level of theory (semiempirical models)[14−18] or obtained by a reduction of the size of the system.[19]

On one hand, density functional theory (DFT) is successful at providing a means to evaluate a variety of ground-state properties with an accuracy close to that of post-HF methods.[20,21] As a consequence, there is currently a great interest in extending DFT to excited electronic states.[22] In this context, the time-dependent DFT (TDDFT) approach offers a rigorous route to the calculation of vertical electronic excitation spectra.[23−25] Furthermore, remarkable structural predictions have been obtained, especially using the "hybrid" density functionals[26,27] such as B3LYP and B3PW91 combining "exact exchange" with gradient-corrected density functionals. For excited states of closed-shell molecules, time-dependent DFT methods (TDDFT)

* To whom correspondence may be addressed. E-mail: Jikangf@ yahoo.com. Fax: +86-431-8945942.

† State Key Laboratory of Theoretical and Computational Chemistry, Institute of Theoretical Chemistry, Jilin University.

‡ The College of Chemistry, Jilin University.

§ Key Lab for Supramolecular Structure and Materials of Ministry of Education, Jilin University.

**6798** *J. Phys. Chem. A, Vol. 108, No. 32, 2004*

Yang et al.

have been developed. Applications of TDDFT approaches have recently been reported on transition-metal complexes and get a considerably good result.[28−31]

On the other hand, Gaussian offers the configuration interaction approach, modeling excited states as combinations of single substitutions out of the HF ground state, and the method is thus named CIS.[32] When paired with a basis set, it also may be used to define excited-state model chemistries whose results may be compared across the full range of practical systems. Theoretical investigations on excited states are uncommon but necessary for the molecules used in organic light-emitting diode devices (OLEDs), because the calculation of excited-state properties typically requires significantly more computational effort than is needed for the ground states.

The structure and electronic properties of the ground and lowest-excited states for the four metal polypyridyl halide complexes ReCl(CO)$_3$(bpy) (**1**), ReCl(CO)$_3$(5,5′-dibromo-bpy) (**2**), ReCl(CO)$_3$(4,4′-dimethyl-bpy) (**3**), and ReCl(CO)$_3$(4,4′-dimethylformyl-bpy) (**4**) have been simulated. The aim of this paper is 2-fold. On one hand, we want to gain information on the physicochemical characteristics of the ground and low-lying excited states and, in particular, to understand the luminescent nature of metal Re complexes and the roles of their different substituents in tuning the dye properties. On the other hand, we want to show the potential of a quantum mechanical modeling based on DFT, in the evaluation of ground- and excited-state properties by comparison to the available experimental data.

## Computation Methods

Calculations on the electronic ground state of four related Re(I) halide complexes **1**, ′**2**, ′**3**, and ′**4** were carried out using B3LYP DFT. The "double-$\xi$" quality basis set LANL2DZ was employed as basis set. A relative effective core potential (ECP) on Re replaced the inner-core electrons, leaving the outer-core [(5s$^2$) (5p$^6$)] electrons and the (5d$^6$) valence electrons of Re(I). The excited-state geometries were optimized at the CIS level of theory. The transition energies will be calculated at the ground-state and excite-state geometries, and the results are compared with the available experimental data. The nature of the excited states, as well as the positive and negative ions with regard to "electron−hole" creation, is relevant to their use in OLED materials. The geometries were fully optimized with $C_s$ symmetry constraints. All calculations are performed with Gaussian 98 using a spin-restricted formalism at the B3LYP/LanL2DZ level of theory, which has proved useful for other rhenium polypyridyl complexes.

## Results and Discussion

The four Re (I) halide complexes **1**, ′**2**, ′**3**, and ′**4** are shown in Figure 1. For the calculated ground-state geometries, the electronic structure is examined in terms of the highest occupied and lowest virtual molecular orbitals. The nature of the low-lying excited states is then explored using the TDDFT approach to derive both absorption and emission spectra, which are compared to available spectroscopic data.

**Ground-State Structures.** The optimized geometrical parameters for all the molecules considered are reported in Table 1, together with the available X-ray data[33] for ′**2**. The calculated structure for complex **2** is depicted in Figure 2 as an example of the four complexes. As depicted, the rhenium(I) in each case adopts a distorted octahedral coordination geometry, and the carbonyl groups are arranged in a facial orientation. All four complexes have similar geometrical rearrangements according
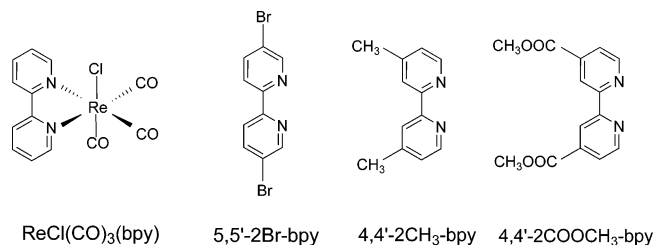


**Figure 1.** Schematic structures of Re(CO)$_3$Cl(bpy) (**1**), Re(CO)$_3$Cl-(5,5′-dibromo-bpy) (**2**), Re(CO)$_3$Cl(4,4′-dimethyl-bpy) (**3**), and Re-(CO)$_3$Cl(4,4′-dimethylformate-bpy) (**4**). The full picture is depicted for parent complex **1**, and for complexes **2**, **3**, and **4** only ligands are depicted.]
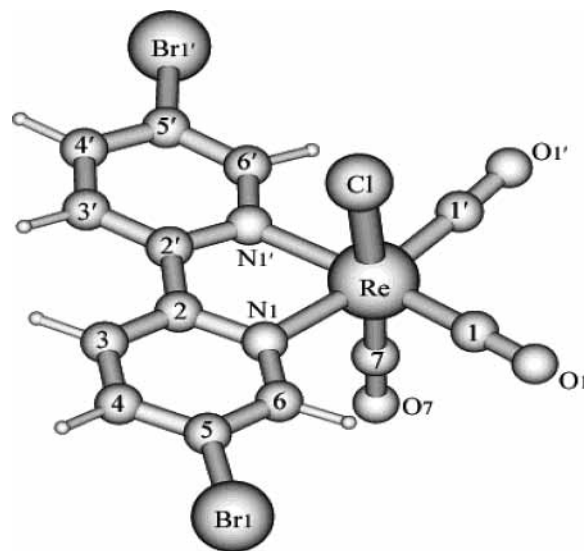


**Figure 2.** The calculated structure for molecule ′**2**.

**TABLE 1: Calculated Bond Lengths for Four Re Center Complexes and the Comparison of Calculated Values with Experimental Values[29] from X-ray Diffraction on the Complexes 2**

| bonds | B3LYP/Å | bonds | B3LYP/Å | exp/Å |
|---|---|---|---|---|
| ReCl(CO)$_3$(bpy) | | ReCl(CO)$_3$(5,5′−2Br-bpy) | | |
| R[Re−N(1)] | 2.172 | R[Re−N(1)] | 2.172 | 2.177 |
| R[Re−N(1′)] | 2.172 | R[Re−N(1′)] | 2.172 | 2.173 |
| R[Re−C(1)] | 1.925 | R[Re−C(1)] | 1.926 | 1.927 |
| R[Re−C(1′)] | 1.925 | R[Re−C(1′)] | 1.926 | 1.951 |
| R[Re−C(7)] | 1.910 | R[Re−C(7)] | 1.912 | 1.917 |
| R[Re−Cl] | 2.548 | R[Re−Cl] | 2.545 | 2.48 |
| ReCl (CO)$_3$(4,4′−2CH$_3$-bpy) | | ReCl (CO)$_3$(4,4′−2COOCH$_3$-bpy) | | |
| R[Re−N(1)] | 2.171 | R[Re−N(1)] | 2.163 | |
| R[Re−N(1′)] | 2.171 | R[Re−N(1′)] | 2.163 | |
| R[Re−C(1)] | 1.925 | R[Re−C(1)] | 1.928 | |
| R[Re−C(1′)] | 1.925 | R[Re−C(1′)] | 1.928 | |
| R[Re−C(7)] | 1.909 | R[Re−C(7)] | 1.913 | |
| R[Re−Cl] | 2.551 | R[Re−Cl] | 2.547 | |

to calculations due to the fact that they have been generated with the same approach and corresponding basis sets and the largest differences concerning bonds to the central metal atom, and these small differences can be attributed to different substituents.

The calculated Re−N bond lengths of 2.172 Å are only 0.005 and 0.001 Å shorter than the experimental values. The Re−C(1), Re−C(1′), and Re−C(7) bond lengths (1.926, 1.926, and 1.912 Å) are about 0.001, 0.025, and 0.005 Å shorter, respectively, than the measured values. The resulting Re−Cl (2.545 Å) bond length differed by 0.065 Å from the experimental values. It seems that the calculated values basically agree with experimental data, except that the axial Re−Cl bond is
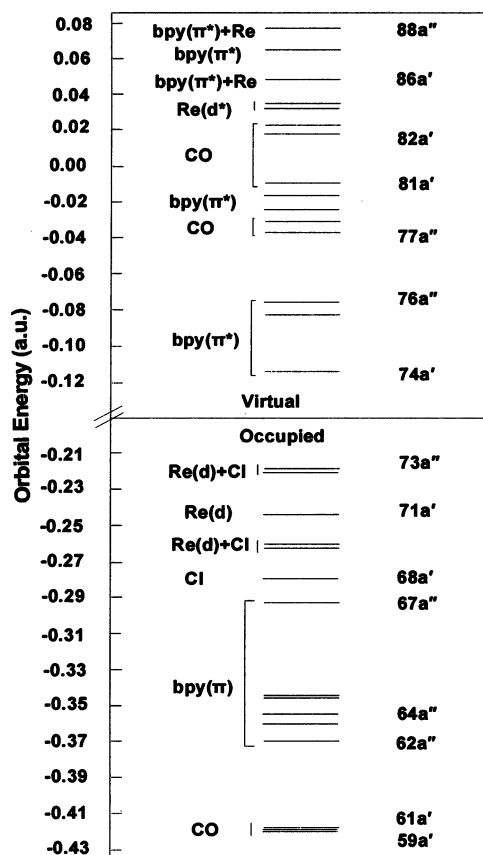
A Series of Halide Rhenium(I) Bipyridine Complexes

*J. Phys. Chem. A, Vol. 108, No. 32, 2004* **6799**



**Figure 3.** Energy-level diagram of Re(CO)₃Cl(bpy) frontier molecular orbitals calculated at the B3LYP/LanL2DZ level. Labels on the left denote the dominant moiety contributing to each molecular orbital. For clarity, only a few of the molecular orbitals are numbered.

overestimated, and this point consists with the research of Turki et al.,[34] in which the author addressed that the drawback of DFT arises from the dynamical correlation effects, which become very important in complexes with a polar Ru−Cl bond. Different substituents slightly influence the bond distances of the molecules. The Re−N(1) and Re−N(1′) bond lengths of the complexes with substituents slightly shortened compared with parent molecule **1**. On the other hand, when substituted by −CH₃, the Re−C(1), Re−C(1′), and Re−C(7) bond lengths are slightly shorter, and when substituted by −Br and −COOCH₃, they are slightly longer than that of parent molecule.

**Molecular Orbitals.** It will be useful to examine the highest occupied and lowest virtual orbitals for these Re complexes to provide the framework for the excited-state TDDFT and CIS calculations in the subsequent section. Moreover, frontier orbitals play a relevant role in such systems because they rule the electronic excitations and the transition character. The frontier orbitals are plotted according to their energies in Figure 3 for complex **1** as an example. The assignment of the type of each MO was made on the basis of its composition (see Table 2, in which only the most important five occupied and three virtual (unoccupied) orbitals are listed) and by visual inspection of its three-dimensional representation (e.g., Figure 4).

We find although the five highest occupied orbitals (HOMOs) have strong rhenium d orbitals (over 30%), nearly equivalent contributions come from the chlorine p orbital, with the exception that the HOMO$_{-2}$ orbitals are mainly rhenium d orbitals, in which the Re d orbital composition exceeds 60% and displays the dominant character. In other words, these occupied MOs are mainly composed of chloride p$_z$ orbitals that form antibonding interactions with metal d$_{xz}$ orbitals (see Table
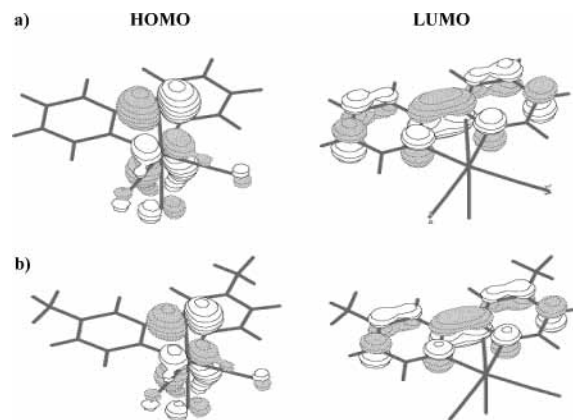


**Figure 4.** Contour plots of highest occupied and lowest virtual orbitals in considered molecules (a) **1** and (b) **3**.

**TABLE 2: Highest Occupied and Lowest Virtual Orbitals with Character for Re Complexes**

| designation | character (%) | $\epsilon$ (au) |
|---|---|---|
| | ReCl(CO)₃(bpy) Occupied | |
| 69 a′ | 5d (37%) + p (Cl) (34%) | −0.262 |
| 70 a″ | 5d (34%) + p (Cl) (39%) | −0.260 |
| 71 a′ | 5d (64%) | −0.245 |
| 72 a′ | 5d (35%) + p (Cl) (37%) | −0.220 |
| 73 a″ (HOMO) | 5d (36%) + p (Cl) (36%) | −0.218 |
| | $\|\Delta E(\text{HOMO}-\text{LUMO})\|^a$ | 0.103 |
| | ReCl(CO)₃(bpy) Virtual | |
| 74 a′ (LUMO) | bpy (93%) | −0.115 |
| 75 a′ | bpy (97%) | −0.082 |
| 76 a″ | bpy (98%) | −0.077 |
| | ReCl(CO)₃(5,5′−2Br-bpy) Occupied | |
| 75 a′ | 5d (33%) + p (Cl) (36%) | −0.270 |
| 76 a″ | 5d (31%) + p (Cl) (38%) | −0.268 |
| 77 a′ | 5d (64%) | −0.253 |
| 78 a′ | 5d (36%) + p (Cl) (38%) | −0.228 |
| 79 a″ (HOMO) | 5d (38%) + p (Cl) (36%) | −0.225 |
| | $\|\Delta E(\text{HOMO}-\text{LUMO})\|^a$ | 0.099 |
| | ReCl(CO)₃(5,5′−2Br-bpy) Virtual | |
| 80 a′ (LUMO) | bpy (89%) | −0.126 |
| 81 a′ | bpy (97%) | −0.095 |
| 82 a″ | bpy (98%) | −0.090 |
| | ReCl (CO)₃(4,4′−2CH₃-bpy) Occupied | |
| 77 a′ | 5d (34%) + p (Cl) (35%) | −0.256 |
| 78 a″ | 5d (33%) + p (Cl) (39%) | −0.255 |
| 79 a′ | 5d (65%) | −0.240 |
| 80 a′ | 5d (36%) + p (Cl) (37%) | −0.215 |
| 81 a″ (HOMO) | 5d (36%) + p (Cl) (36%) | −0.213 |
| | $\|\Delta E(\text{HOMO}-\text{LUMO})\|^a$ | 0.105 |
| | ReCl (CO)₃(4,4′−2CH₃-bpy) Virtual | |
| 82 a′ (LUMO) | bpy (91%) | −0.107 |
| 83 a′ | bpy (95%) | −0.074 |
| 84 a″ | bpy (95%) | −0.066 |
| | ReCl (CO)₃(4,4′−2COOCH₃-bpy) Occupied | |
| 99 a′ | 5d (37%) + p (Cl) (33%) | −0.268 |
| 100 a″ | 5d (35%) + p (Cl) (38%) | −0.266 |
| 101 a′ | 5d (64%) | −0.251 |
| 102 a′ | 5d (34%) + p (Cl) (38%) | −0.226 |
| 103 a″ (HOMO) | 5d (35%) + p (Cl) (37%) | −0.224 |
| | $\|\Delta E(\text{HOMO}-\text{LUMO})\|^a$ | 0.092 |
| | ReCl (CO)₃(4,4′−2COOCH₃-bpy) Virtual | |
| 104 a′ (LUMO) | bpy (78%) + p (COOCH₃) | −0.132 |
| 105 a″ | bpy (70%) + p (COOCH₃) | −0.111 |
| 106 a′ | bpy (92%) + p (COOCH₃) | −0.096 |

$^a$ $\Delta E$ refers to band gap.

2 and Figure 3). Some lower-energy occupied MOs are mainly centered on the bpy ligands or group CO in each complex. On one hand, Turki and co-worker[34] calculated the UV−vis

**TABLE 3: Ionization Potentials, Electron Affinities, "Small-Polaron" Stabilization Energies, and Spin Densities for the Four Complexes (in eV)[a]**

| | | | | | | | spin density of cation (%) | | | | |
|---|---|---|---|---|---|---|---|---|---|---|---|
| | IP(v) | IP(a) | HEP | SPE(h) | Re | bpy | 3CO | Cl | 2Br | 2CH₃ | 2COOCH₃ |
| **1** | 7.59 | 7.36 | 0.23 | 0.23 | 0.53 | 0.02 | 0.10 | 0.35 | | | |
| **2** | 7.80 | 7.57 | 0.23 | 0.23 | 0.54 | 0.03 | 0.09 | 0.32 | 0.02 | | |
| **3** | 7.43 | 7.19 | 0.25 | 0.24 | 0.54 | 0.03 | 0.10 | 0.33 | | 0.00 | |
| **4** | 7.67 | 7.42 | 0.24 | 0.25 | 0.52 | 0.01 | 0.10 | 0.37 | | | 0.00 |

| | | | | | | | spin density of anion (%) | | | | |
|---|---|---|---|---|---|---|---|---|---|---|---|
| | EA(v) | EA(a) | EEP | SPE(e) | Re | bpy | 3CO | Cl | 2Br | 2CH₃ | 2COOCH₃ |
| **1** | −1.63 | −1.84 | 0.21 | 0.21 | −0.01 | 0.96 | 0.04 | 0.01 | | | |
| **2** | −2.04 | −2.21 | 0.17 | 0.17 | −0.01 | 0.95 | 0.04 | 0.02 | 0.00 | | |
| **3** | −1.49 | −1.72 | 0.23 | 0.22 | −0.01 | 0.95 | 0.04 | 0.01 | | 0.01 | |
| **4** | −2.28 | −2.50 | 0.22 | 0.22 | −0.00 | 0.76 | 0.03 | 0.01 | | | 0.20 |

[a] See text for definitions. The suffixes v and a respectively indicate vertical and adiabatic values.

absorption spectra of the Ru complex containing Cl with CASSCF/CASPT2 and TDDFT methods; they thought DFT calculations overestimate halide contributions in metal−halide complexes, especially if a low valent metal atom is involved, although DFT approaches are remarkably good in the case of nonhalide complexes. On the other hand, Stufkens[35,36] have analyzed that the electronic transitions to the α-diimine have strongly mixed metal-to-ligand charge transfer (MLCT)/X-to-ligand charge transfer (XLCT) character due to the interaction of M−$d_\pi$ and X−$p_\pi$ orbitals in experiment. As a result, two absorption bands are observed, the relative intensities of which depend on the metal character of the orbitals involved in the transitions. In contrast, the LUMO and two subsequent virtual (unoccupied) orbitals are essentially $\pi^*$ orbitals localized on the bipyridine moieties (over 90%), but the higher LUMOs show considerable localization on the CO groups. The four other rhenium orbitals (MO 84a″, MO 85a′, MO 86a′, and MO 88a″) with mainly d character are still higher in energy and display nobonding or antibonding interactions with the ligands. However, since the contribution from these orbitals is quite small for low-energy transition, we only concentrate on the orbitals listed in Table 2. In fact, due to their similar basic structure, the frontier orbitals have similar features in all the considered complexes.

For intuition, the contour plot of HOMO and LUMO orbitals for molecules **1** and **3** are depicted as example in Figure 4. In the contour plots, the mixing of 5d (Re) and Cl (p) is evident, while the LUMO is seen to be delocalized over the bpy ligand. Thus there must be a mixture between MLCT and ligand-to-ligand charge transfer (LLCT) upon transition from the ground state to the excited state.

But different substituents still influence the character of the complexes as shown in Table 2. We note that the three lowest unoccupied orbitals are essentially $\pi^*$ orbitals of the bipyridine moieties, whereas the substituents are localized at bipyridine rings. So substituents have a direct effect on LUMO. From the energies listed, we observed that the electron-releasing −CH₃ group slightly increases the LUMO energy, resulting in the increased HOMO−LUMO band gap, which then leads to a decrease in the $\lambda_{max}$ values. On the other hand, electron-withdrawing −Br and −COOCH₃ groups decrease the LUMO energy, resulting in the decreased band gap in the order −Br > −COOCH₃, which then leads to an increase in the $\lambda_{max}$ values.

**Ionization Potentials and Electron Affinities.** Additional information derived from our calculations provides insight into the inter-relationship of structure and electronic behavior, in particular the response of the molecule to the formation of a hole or the addition of an electron. Table 3 contains the ionization potentials (IPs), electron affinities (EAs), both vertical (v, at the geometry of the neutral molecule) and adiabatic (a, optimized structure for both the neutral and charged molecule), and extraction potentials (HEP and EEP for the hole and the electron, respectively) that refer to the geometry of the ions. Relatively small energy changes are associated with structural relaxation. In all cases, the energy required to create a hole is ~8 eV, while the extraction of an electron from the anion requires ~2 eV. In fact, these complexes share the common features of having accessible Re-based oxidations and bipyridine-based reductions. In fact, early work has amply demonstrated that ReX(CO)₃(diimine) complexes are both strong reductants and oxidants. Experimental research reveals nearly reversible oxidation and reduction waves at ~+1.3 and ~−1.3 V vs an aqueous saturated calomel electrode for the complex *fac*-ReCl(CO)₃(phen).[37] It is found that the calculated IPs (no matter IP(a) or IP(v)) of molecules **2** and **4** are relatively larger, whereas for molecule **3**, they are relatively lower than their parent molecule, which is in agreement with the trend in HOMO energy. These all correspond to removal of an electron from the "5d" orbital. As shown in the cation spin densities in Table 3, over 50% of the spin density in all four complexes is on the Re and the remainder largely shared on group Cl and less on bpy and CO ligands, which means there will be mixed character between metal Re and group Cl for electronic transitions, and this basically consists of the analysis of HOMO composition.

Four complexes show weakly bound negative ions, corresponding to the electron affinity. In each complex, the unpaired spin density are totally on bpy ligands and less on CO and Cl ligands. This is consistent with the LUMO being primarily the bpy $\pi^*$ orbitals. Although both IP(a) and EA(a) are lower than 0.23 eV on average than IP(v) and EA(v), respectively, due to structural relaxation after oxidation or reduction, the structure changes little after electron reduction or addition.

The same calculations are also used to estimate self-trapping energies of positive and negative charges in the materials. Indeed, in ref 38, the traps that characterize the electron transport in the material were identified as the states in which the injected electron is self-trapped in the individual molecules as a consequence of structure relaxation. Such a procedure, however, provides an estimate of the exciton trap energy rather than that of the injected electron. Following the same interpretation for the trap states, the correct energy in our scheme is the energy gain of the excess electron due to structural relaxation, i.e., the difference EA(a) − EA(v), which we also report in Table 3, as the "small-polaron" stabilization energy (SPE) for the electron. It seems that the four complexes appear to trap the electron nearly the same efficiently. The SPE values may be compared

A Series of Halide Rhenium(I) Bipyridine Complexes

*J. Phys. Chem. A, Vol. 108, No. 32, 2004* **6801**

**TABLE 4: Selected Calculated Excitation Energies ($E$), Wavelengths ($\lambda$), Oscillator Strenghs ($\times$c4), and Dominant Excitation Character for Low-Lying Singlet ($S_n$) and Triplet ($T_n$) States of the Complex ReCl(CO)$_3$(bpy) and Comparison with Experimental Data**

| state | excitation | $E_{cal}$, eV | $\lambda_{cal}$, nm | $\times$c4$_{cal}$ | $\lambda_{exp}$, nm | character |
|---|---|---|---|---|---|---|
| | | | Singlet Excited States | | | |
| 1(A″) | 73 → 74(0.70) | 2.04 | 609 | 0.0013 | | MLCT/LLCT |
| 2(A′) | 72 → 74(0.68) | 2.21 | 561 | 0.0315 | | MLCT/LLCT |
| 9(A′) | 69 → 74(0.64) | 3.35 | 370 | 0.0872 | 387(CH$_2$Cl$_2$) | MLCT/LLCT |
| | | | | | 370(CH$_3$CN)[37] | |
| 14(A′) | 73 → 77(0.58) | 3.93 | 315 | 0.0103 | | MLCT/LLCT |
| 17(A′) | 69 → 75(0.65) | 4.23 | 293 | 0.0134 | | MLCT/LLCT |
| 18(A″) | 69 → 76(0.58) | 4.28 | 290 | 0.0228 | | MLCT/LLCT |
| | 67 → 74(0.32) | | | | | LLCT |
| 19(A′) | 72 → 78(0.56) | 4.30 | 288 | 0.0185 | | MLCT/LLCT |
| | 73 → 77(0.17) | | | | | MLCT/LLCT |
| 20(A′) | 70 → 76(0.65) | 4.35 | 285 | 0.0614 | | MLCT/LLCT |
| | 69 → 75(0.19) | | | | | MLCT/LLCT |
| 21(A′) | 73 → 79(0.69) | 4.53 | 274 | 0.0160 | | MLCT/LLCT |
| 22(A″) | 67 → 74(0.43) | 4.54 | 273 | 0.2318 | 293(CH$_2$Cl$_2$) | IL |
| | 69 → 76(0.33) | | | | | MLCT/LLCT |
| | 71 → 77(0.26) | | | | | MLCT |
| 25(A″) | 72 → 80(0.45) | 4.71 | 263 | 0.1202 | | MLCT/LLCT |
| | 71 → 77(0.31) | | | | | MLCT |
| | 72 → 79(0.28) | | | | | MLCT/LLCT |
| 27(A″) | 68 → 76(0.69) | 4.86 | 255 | 0.0301 | | LLCT |
| 28(A″) | 72 → 80(0.40) | 4.90 | 253 | 0.0372 | | MLCT/LLCT |
| | 71 → 80(0.30) | | | | | MLCT |
| | 73 → 81(0.24) | | | | | MLCT/LLCT |
| 29(A′) | 73 → 80(0.52) | 4.95 | 251 | 0.0168 | | MLCT/LLCT |
| | 69 → 78(0.26) | | | | | MLCT/LLCT |
| 33(A″) | 67 → 75(0.53) | 5.17 | 240 | 0.0827 | | IL |
| | 65 → 74(0.25) | | | | | IL |
| 34(A″) | 70 → 78(0.41) | 5.18 | 239 | 0.0250 | | MLCT/LLCT |
| | 71 → 79(0.29) | | | | | IL |
| 35(A′) | 67 → 76(0.53) | 5.22 | 238 | 0.0157 | | IL |
| | 72 → 81(0.24) | | | | | MLCT/LLCT |
| | 64 → 74(0.21) | | | | | IL |
| 40(A″) | 72 → 83(0.49) | 5.46 | 227 | 0.0230 | | MLCT/LLCT |
| | 71 → 80(0.31) | | | | | MLCT |
| | | | Triplet Excited States | | | |
| 1(A″) | 73 → 74(0.71) | 1.97 | 628 | 0.0000 | | MLCT/LLCT |
| 2(A′) | 72 → 74(0.71) | 2.03 | 610 | 0.0000 | | MLCT/LLCT |
| 3(A′) | 71 → 74(0.71) | 2.71 | 457 | 0.0000 | | MLCT |
| 4(A″) | 70 → 74(0.52) | 2.86 | 434 | 0.0000 | | MLCT/LLCT |
| | 67 → 74(0.40) | | | | | IL |
| 5(A″) | 73 → 75(0.69) | 2.98 | 416 | 0.0000 | | MLCT/LLCT |

with tris-(8-hydroxyquinolate)-aluminum (Alq) another dopant for OLED applications. Similar DFT calculations[39] on Alq predicted 0.13 eV for SPE.

**Excitation Energies.** With the prerequisite ground-state DFT calculation in hand, we proceed to the time-dependent calculation of complexes **1**−**4** to find the characters and energies of their low-lying singlet and triplet excited states. We begin with the singlet → singlet spin-allowed transition. Forty singlet excited states are calculated at the optimized structure of the ground state for each complex, and only the singlet excited states with the greatest oscillator strengths (above 0.01) are typically listed in Tables 4−7, together with experimental data; this information is also presented graphically for all calculated excited states in Figures 6−9, respectively. The energy of each excited is vertical excitation energy in eV from the ground state. As shown, the four complexes have relatively similar absorption character. There are significant oscillator strength throughout the ∼2−5-eV region, but there are also several singlet excited states with zero oscillator strength, and these states, although present in the molecule's excited-state manifold, will therefore no contribute to the compound's absorption spectra. No excited states or absorption features are found below 1 eV.

A commonly used model of an excited state corresponds to excitation of an electron from an occupied to a virtual MO (i.e.,

a one-electron picture). However, the excited states calculated herein demonstrate that excited-state electronic structures are best described in terms of multiconfigurations, wherein a linear combination of several occupied-to-virtual MO excitations comprises a given optical transition. Assignment of the character of each excited state was based on the compositions of the occupied and virtual MOs of the dominant configuration(s) for that excited state. We selected complex **1** shown in Table 4 as analysis example. For the $T_3$ excited state, the dominant excitation is 71 → 74, and since the occupied orbital (71) is metal based and the virtual orbital (74) is bipyridine $\pi^*$, the transition is designated as a MLCT. Similarly, for the $S_{27}$ excited state, the dominant excitation is 68 → 76, and since the occupied orbital (68) is localized on a halide chlorine and virtual orbital (76) type is bipyridine $\pi^*$, the transition is designated as a LLCT. For $S_{33}$, the dominant excitation is from bipyridine $\pi$ (65 and 67) to bipyridine $\pi^*$ (74 and 75), the transition is designated as intraligand (IL) character. After presenting the detailed theoretical results is this section, in the following section, we summarize the excited states for the four complexes and compare them to experimental absorption and emission studies.

Figure 5 illustrates the differences of MLCT, LLCT, and IL excitations for three strongly allowed transitions of complex **1**.
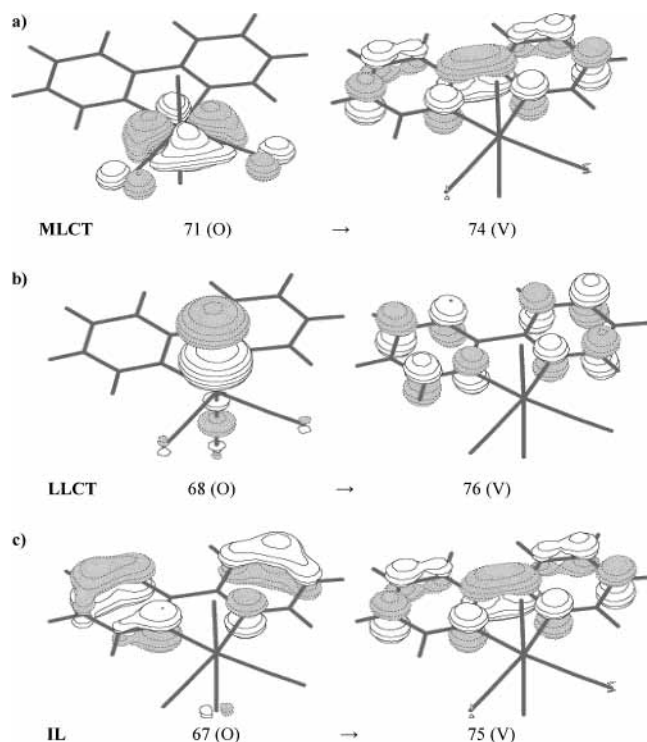
**Figure 5.** Example of dominant occupied and virtual orbitals for three different types of excitations of complex **1**. (a) MLCT excitation (71 → 74). (b) LLCT excitation (68 → 76). (c) IL excitation (67 → 75).

Moreover, for the $S_1$ excited state, the calculated spin density of positive and negative ions also has significant referenced values for transition assignment. For the majority of the excited states calculated, such an assignment can be made unambiguously. However, for the metal−halide molecules under studying

on, most of the significant excited states exhibit mixed MLCT and LLCT and, sometimes, IL characters. In fact, excited-state character as a function of the molecular structure has been reviewed form the experimental point of view, such as in the ref 34 where the author addressed that the character of the lowest excited states changes gradually from MLCT to LLCT while halide ligand changes from Cl to Br, especially, to I in Re(E)-(CO)$_3$(α-diimine) complexes, which are consistent with our calculations.

From Tables 4−7 and Figures 6−9, we see that in each complex the low-energy part of the absorption spectra originated in an electronic transition that corresponds to excitation from the rich mixed orbitals of metal Re and chlorine Cl into π* orbital localized predominantly on bpy. And the intense bands are observed at a relative higher-energy region, which corresponds to ππ* excitations. Furthermore, we compare the results of the excited states of **2**, **3**, and **4** with **1**. From the earlier discussion of the frontier orbitals (Table 2 and Figure 3), due to the influence of the electron-releasing or withdrawing substituents, the energy gaps ($|\Delta E$(HOMO−LUMO)$|$) decrease in the order 3 > 1 > 2 > 4, and this rule remains constant in absorption spectra. The absorption bands exhibit blue shifts in **2** and red shifts in **3** and **4** compared with **1**. It is evident for $S_1$, where 2.12 (−CH$_3$) > 2.04 > 1.93 (−Br) > 1.75 eV (−COOCH$_3$). But the band character basically is identical.

The 35 lowest-energy triplet excited states were also calculated, using analogous TDDFT methodology. The first five triplet excited states are listed in Table 2. MLCT, LLCT, and IL excited states are all seen, but most of them are the mixed character, as with the singlets. As expected from Hund's rule, transitions to the triplet states tend to be lower in energy than their corresponding singlets. For example, in complex **1**, the first triplet vertical transition energy is 1.97 eV lower than that of the first singlet excited state (2.04 eV), where both represent

**TABLE 5: Selected Calculated Excitation Energies ($E$), Wavelengths ($\lambda$), Oscillator Strenghs ($\times$c4), and Dominant Excitation Character for Low-Lying Singlet ($S_n$) and Triplet ($T_n$) States of the Complex ReCl(CO)$_3$(5,5′-2Br-bpy) and Comparison with Experimental Data.**

| state | excitation | $E_{cal}$, eV | $\lambda_{cal}$, nm | $\times$c4$_{cal}$ | $\lambda_{exp}$, nm | character |
|---|---|---|---|---|---|---|
| | | | Singlet Excited States | | | |
| 1(A″) | 79 → 80(0.70) | 1.93 | 643 | 0.0012 | | MLCT/LLCT |
| 2(A′) | 78 → 80(0.68) | 2.12 | 585 | 0.0310 | | MLCT/LLCT |
| 9(A′) | 75 → 80(0.66) | 3.26 | 381 | 0.0814 | 410(CH$_2$Cl$_2$) | MLCT/LLCT |
| 13(A″) | 74 → 80(0.46) | 3.88 | 320 | 0.1518 | 316(CH$_2$Cl$_2$) | IL |
| | 76 → 81(0.29) | | | | | MLCT/LLCT |
| 15(A″) | 78 → 83(0.52) | 3.89 | 319 | 0.0582 | | MLCT/LLCT |
| | 74 → 80(0.28) | | | | | IL |
| 17(A″) | 76 → 81(0.58) | 4.06 | 306 | 0.1319 | | MLCT/LLCT |
| | 75 → 82(0.26) | | | | | MLCT/LLCT |
| 18(A′) | 75 → 81(0.64) | 4.10 | 302 | 0.0105 | | MLCT/LLCT |
| 19(A′) | 76 → 82(0.63) | 4.20 | 295 | 0.0629 | | MLCT/LLCT |
| | 75 → 81(0.20) | | | | | MLCT/LLCT |
| 20(A′) | 78 → 84(0.53) | 4.23 | 293 | 0.0232 | | MLCT/LLCT |
| | 78 → 87(0.25) | | | | | MLCT/LLCT |
| 21(A″) | 75 → 82(0.57) | 4.27 | 290 | 0.1933 | | MLCT/LLCT |
| | 79 → 87(0.16) | | | | | MLCT/LLCT |
| 22(A″) | 79 → 84(0.48) | 4.31 | 288 | 0.0551 | | MLCT/LLCT |
| | 75 → 82(0.22) | | | | | MLCT/LLCT |
| 23(A′) | 79 → 85(0.64) | 4.37 | 284 | 0.0189 | | MLCT/LLCT |
| 31(A″) | 74 → 81(0.62) | 4.65 | 267 | 0.1082 | 256(CH$_2$Cl$_2$) | IL |
| 32(A″) | 77 → 83(0.44) | 4.65 | 266 | 0.0634 | | MLCT |
| | 78 → 88(0.39) | | | | MLCT/LLCT | |
| 33(A″) | 73 → 82(0.69) | 4.70 | 264 | 0.0159 | | IL |
| 34(A′) | 74 → 82(0.61) | 4.77 | 256 | 0.0297 | | IL |
| | | | Triplet Excited States | | | |
| 1(A″) | 79 → 80(0.71) | 1.87 | 664 | 0.0000 | | MLCT/LLCT |
| 2(A′) | 78 → 80(0.72) | 1.93 | 642 | 0.0000 | | MLCT/LLCT |
| 3(A′) | 77 → 80(0.71) | 2.61 | 474 | 0.0000 | | MLCT |
| 4(A″) | 76 → 80(0.62) | 2.69 | 460 | 0.0000 | | MLCT/LLCT |
| 5(A″) | 79 → 81(0.70) | 2.83 | 438 | 0.0000 | | MLCT/LLCT |

A Series of Halide Rhenium(I) Bipyridine Complexes

*J. Phys. Chem. A, Vol. 108, No. 32, 2004* **6803**

**TABLE 6: Selected Calculated Excitation Energies (E), Wavelengths (λ), Oscillator Strenghs (×c4), and Dominant Excitation Character for Low-Lying Singlet (S_n) and Triplet (T_n) States of the Complex ReCl (CO)_3(4,4′-2CH_3-bpy) and Comparison with Experimental Data**

| state | excitation | $E_{cal}$, eV | $\lambda_{cal}$, nm | $\times c4_{cal}$ | $\lambda_{exp}$, nm | character |
|---|---|---|---|---|---|---|
| | | | Singlet Excited States | | | |
| 1(A″) | 81 → 82(0.70) | 2.12 | 586 | 0.0013 | | MLCT/LLCT |
| 2(A′) | 80 → 82(0.69) | 2.28 | 544 | 0.0347 | | MLCT/LLCT |
| 9(A′) | 77 → 82(0.59) | 3.39 | 365 | 0.0954 | 380(CH_2Cl_2) | MLCT/LLCT |
| | 81 → 84(0.33) | | | | 364(CH_3CN)[37] | MLCT/LLCT |
| 13(A′) | 81 → 85(0.47) | 3.95 | 314 | 0.0111 | | MLCT/LLCT |
| | 76 → 82(0.44) | | | | | LLCT |
| 17(A′) | 77 → 83(0.57) | 4.28 | 290 | 0.0203 | | MLCT/LLCT |
| | 81 → 88(0.16) | | | | | MLCT/LLCT |
| 18(A′) | 80 → 86(0.46) | 4.31 | 288 | 0.0257 | | MLCT/LLCT |
| | 77 → 83(0.37) | | | | | MLCT/LLCT |
| 19(A″) | 77 → 84(0.54) | 4.36 | 284 | 0.0454 | | MLCT/LLCT |
| | 75 → 82(0.36) | | | | | IL |
| 20(A′) | 78 → 84(0.66) | 4.45 | 279 | 0.0521 | 290(CH_2Cl_2) | MLCT/LLCT |
| | 81 → 87(0.18) | | | | | MLCT/LLCT |
| 21(A′) | 81 → 87(0.67) | 4.55 | 272 | 0.0281 | | MLCT/LLCT |
| 22(A″) | 80 → 87(0.51) | 4.57 | 271 | 0.0186 | | MLCT/LLCT |
| | 79 → 85(0.32) | | | | | MLCT |
| 24(A″) | 80 → 87(0.38) | 4.59 | 270 | 0.1698 | | MLCT/LLCT |
| | 75 → 82(0.36) | | | | | LLCT |
| 25(A″) | 80 → 88(0.43) | 4.71 | 263 | 0.1773 | 260(CH_2Cl_2) | MLCT/LLCT |
| | 80 → 87(0.30) | | | | | MLCT/LLCT |
| | 79 → 85(0.15) | | | | | MLCT |
| 27(A″) | 80 → 88(0.40) | 4.90 | 253 | 0.0640 | | MLCT/LLCT |
| | 81 → 89(0.21) | | | | | MLCT/LLCT |
| 28(A′) | 81 → 88(0.51) | 4.95 | 251 | 0.0171 | | MLCT/LLCT |
| | 80 → 90(0.19) | | | | | MLCT/LLCT |
| | 80 → 86(0.18) | | | | | MLCT/LLCT |
| 29(A″) | 76 → 84(0.68) | 4.98 | 249 | 0.0110 | | LLCT |
| 33(A″) | 75 → 83(0.49) | 5.12 | 242 | 0.0674 | | IL |
| | 74 → 82(0.39) | | | | | IL |
| 40(A″) | 80 → 91(0.45) | 5.46 | 227 | 0.0302 | | LLCT |
| | 79 → 88(0.32) | | | | | MLCT |
| | 78 → 86(0.22) | | | | | MLCT/LLCT |
| | | | Triplet Excited States | | | |
| 1(A″) | 81 → 82(0.71) | 2.06 | 602 | 0.0000 | | MLCT/LLCT |
| 2(A′) | 80 → 82(0.71) | 2.12 | 586 | 0.0000 | | MLCT/LLCT |
| 3(A′) | 79 → 82(0.70) | 2.79 | 444 | 0.0000 | | MLCT |
| 4(A″) | 78 → 82(0.52) | 2.89 | 429 | 0.0000 | | MLCT/LLCT |
| | 75 → 82(0.43) | | | | | IL |
| 5(A′) | 77 → 82(0.50) | 3.04 | 408 | 0.0000 | | MLCT/LLCT |
| | 80 → 83(0.44) | | | | | MLCT/LLCT |

(predominantly) a MO 73 → MO 74 transition. The TDDFT results do not provide information on triplet–singlet absorption intensities since spin–orbit coupling effects are not included in current TDDFT approaches, which is the reason the oscillator strengths in triplet excited states are all zero. Spin–orbit coupling can mix singlet and triplet states, allowing the latter to acquire intensity in both absorption and emission. A second effect is that the triplet energies are shifted through coupling with higher singlet (or other triplet) states. For third-row transition metals, one[40] estimates the lowest triplet states to be lowered by ∼0.2–0.3 eV from interactions with higher states through spin–orbital coupling. The TDDFT results should still provide a reasonable description of the overall orbital excitations that would be coupled in a subsequent spin–orbit treatment.

**Comarison with Experimental Results.** Combined with experimental data gathered over time, computed spectra may provide a reference for monitoring the behavior and possible degradation of the organic material in the device. The results of the TDDFT calculations for complexes **1**–**4** are compared with experimental absorption data (see Tables 4–7) and are depicted in Figures 6–9. The spectral assignment is based on a comparison of experimental band maxima with calculated energies of transitions with significant oscillator strengths,

including the simulated spectra figures. The principal experimental studies cited in the table have been carried out by Ming Zhang et al. in the Key Lab for Supramolecular Structure and Materials of Ministry of Education at Jilin University.

To independently check that these calculations produce reasonable results, the absorption spectra of the four complexes are simulated based on the TDDFT calculations (Figure 6–9). Here, each excited-state having ×c4 ≥ 0 (as shown in Tables 4–7) was modeled as a Gaussian feature in the program OriginPro70. The numbers of maximum peaks in a certain region are decided as the number of peaks. Selection of the initial half-width estimate of each Gaussian was based upon the default values. Each graph of calculated molar absorptivity (Figures 6–9) shows a Gaussian corresponding to each of the 40 calculated singlet excited states. For example, for complex **1**, starting from the lowest transition calculated at 609 nm to 227 nm are taken into the simulation. It seems that the simulated spectra are all in reasonable agreement with the experimental spectrum. In fact, there have been numerous spectroscopic studies on Re(I) bpy complexes. Meyer and co-workers[41] reported the near-UV–vis absorption spectrum of the "model" complex, (4,4′-X_2-2,2′-bipyrdine)Re(CO)_3Cl. The absorption maxima are at relatively high energy and overlap with bpy-

**TABLE 7: Selected Calculated Excitation Energies ($E$), Wavelengths ($\lambda$), Oscillator Strengths ($\times c4$), and Dominant Excitation Character for Low-Lying Singlet ($S_n$) and Triplet ($T_n$) States of the Complex ReCl (CO)$_3$(4,4′-2COOCH$_3$-bpy) and Comparison with Experimental Results**

| state | excitation | $E_{cal}$, eV | $\lambda_{cal}$, nm | $\times c4_{cal}$ | $\lambda_{exp}$, nm | character |
|---|---|---|---|---|---|---|
| | | | Singlet Excited States | | | |
| 1(A″) | 103 →104(0.70) | 1.75 | 707 | 0.0040 | | MLCT/LLCT |
| 2(A′) | 102 →104(0.67) | 1.95 | 635 | 0.0369 | | MLCT/LLCT |
| 4(A′) | 103 →105(0.53) | 2.48 | 500 | 0.0136 | | MLCT/LLCT |
| | 101 →104(0.34) | | | | | MLCT |
| 5(A″) | 102 →105(0.70) | 2.53 | 489 | 0.0211 | | MLCT/LLCT |
| 9(A′) | 99 →104(0.66) | 3.10 | 400 | 0.1237 | 433(CH$_2$Cl$_2$) | MLCT/LLCT |
| 13(A″) | 99 →105(0.68) | 3.65 | 340 | 0.0217 | | MLCT/LLCT |
| 14(A′) | 100 →105(0.68) | 3.67 | 338 | 0.1110 | | MLCT/LLCT |
| 15(A″) | 100 →106(0.57) | 3.90 | 318 | 0.0379 | | MLCT/LLCT |
| 19(A′) | 99 →106(0.67) | 4.01 | 309 | 0.0326 | | MLCT/LLCT |
| 22(A″) | 97 →104(0.41) | 4.12 | 301 | 0.1688 | 313(CH$_2$Cl$_2$) | IL |
| | 100 →106(0.35) | | | | | MLCT/LLCT |
| 23(A″) | 98 →105(0.60) | 4.16 | 298 | 0.1244 | | MLCT/LLCT |
| | 97 →104(0.26) | | | | | IL |
| 25(A′) | 102 →109(0.57) | 4.28 | 290 | 0.0169 | | MLCT/LLCT |
| | 103 →108(0.23) | | | | | MLCT/LLCT |
| 29(A′) | 97 →105(0.50) | 4.57 | 271 | 0.0149 | | IL |
| | 98 →106(0.33) | | | | | MLCT/LLCT |
| 30(A″) | 102 →111(0.49) | 4.66 | 266 | 0.0159 | | MLCT/LLCT |
| | 101 →108(0.39) | | | | | MLCT |
| 35(A″) | 102 →111(0.42) | 4.90 | 253 | 0.0120 | | MLCT/LLCT |
| | 103 →112(0.19) | | | | | MLCT/LLCT |
| 37(A′) | 102 →110(0.45) | 5.03 | 246 | 0.0190 | | MLCT/LLCT |
| | 99 →109(0.19) | | | | | MLCT/LLCT |
| | 100 →108(0.18) | | | | | MLCT/LLCT |
| 38(A″) | 97 →106(0.67) | 5.04 | 246 | 0.1942 | | IL |
| | | | Triplet Excited States | | | |
| 1(A″) | 103 → 104(0.71) | 2.06 | 602 | 0.0000 | | MLCT/LLCT |
| 2(A′) | 102 → 104(0.72) | 2.12 | 586 | 0.0000 | | MLCT/LLCT |
| 3(A′) | 103 → 105(0.70) | 2.79 | 444 | 0.0000 | | MLCT/LLCT |
| 4(A′) | 101 → 104(0.71) | 2.89 | 429 | 0.0000 | | MLCT |
| 5(A″) | 100 → 104(0.69) | 3.04 | 408 | 0.0000 | | MLCT/LLCT |

based, $\pi\pi^*$ bands. The lowest energy absorption band (or shoulder) is assigned to a MLCT transition (Re$^l$ → bpy). The MLCT absorption spectra are sensitive to the nature of the substituents on the polypyridyl ligand. The electron-donating substituents increase the energy of the $\pi^*$ (4, 4′-X$_2$-bpy) acceptor orbitals to a greater degree than they do the d$\pi$ (Re) orbitals. At the same time, Keith et al.[13] thought that the absorption bands for complex ReCl(CO)$_3$(4,4′-{bis-[2,5-(dimethoxyphenyl)ethynyl]}-2,2′-bipyridine) are dominated by IL $\pi\pi^*$ transitions although the low-energy absorption band contains a contribution from an MLCT transition. They considered there is configuration interaction between the IL $\pi\pi^*$ and MLCT transitions, and because of such configuration interactions, the low-energy transition will have characteristics that are a composite of the two transitions.

For ReCl(CO)$_3$(bpy), the calculated excitation energy (3.35 eV) with strong intensity (0.0872) for S$_9$ (A′) arising from the mixed MLCT d → $\pi^*$ (bpy)/LLCT p → $\pi^*$ (bpy) excitation is close to the onset of absorption (3.20 eV, 387 nm). Experimentally, this band was assigned to MLCT d → $\pi^*$ (bpy); TDDFT results label this mixed character. This should be qualified by the fact that 5d orbitals are highly mixed with p character on the halide Cl as discussed earlier. The other higher-energy absorption peaks at 4.23 eV (293 nm) occur in the same region of a singlet state S$_{22}$ (A″) calculated at 4.54 eV with large oscillator strength, which corresponds to $\pi\pi^*$ excitation and considerable MLCT/LLCT. In general, the simulated spectra exhibit slight blue shifts compared with experimental ones.

For ReCl(CO)$_3$(4,4′-2Br-bpy), the two relative higher-energy absorption at 256 (4.84) and 316 nm (3.92 eV) corresponds to $\pi\pi^*$ excitation, and the latter mix considerable MLCT/LLCT,

at calculated values of 293 (4.23) and 320 nm (3.88 eV) from S$_{21}$(A″) and S$_{13}$(A″), respectively. The absorption peak at 410 nm (3.02 eV) agrees well with the lower singlet state S$_9$ (A′) arising from d (Re) and p (Cl) to $\pi^*$ (bpy) excitation (3.26 eV).

From Figure 3b, we noted that at nearly 250−260 nm, there exists one shoulder peak at 260 nm (4.76 eV) observed in experiment for ReCl (CO)$_3$(4,4′-2CH$_3$-bpy), but because in this region the oscillator strength is similar, it cannot present in the simulated spectra. We still assign it to mixed MLCT/LLCT character arising from S$_{25}$ (A″). High-energy absorption peaks at 290 nm (4.28 eV) occur in the same region of S$_{20}$ (A′), and the low-energy ones at 380 nm (3.26 eV) correspond to S$_9$ (A′), and they both arise from MLCT d → $\pi^*$ (bpy)/LLCT p → $\pi^*$ (bpy).

ReCl (CO)$_3$(4,4′-2COOCH$_3$-bpy) have two absorption bands. The low-energy one at 432 nm (2.87 eV) corresponds to S$_9$ (A′) at 400 nm (3.10 eV) arising from MLCT d → $\pi^*$ (bpy)/LLCT p → $\pi^*$ (bpy). The other calculated broad one 313 nm (3.96 eV) corresponds to S$_{22}$ (A″) at 301 nm (4.12 eV) arising from IL excitation with considerable MLCT/LLCT. The calculated absorption bands exhibit slight blue shifts compared with experiment.

Furthermore, the spectra illustrate the considerable effect that different substituents at the chromophoric ligand have on the spectral properties of the complexes. The main bands are red shifted in the complexes substituted by the electron-withdrawing groups −Br and −COOCH$_3$ and blue shifted in the electron-releasing group −CH$_3$ substituted complex. This variation is consistent with the orbital characters analyzed above.

**Lowest Triplet States.** The lowest triplet states of the four molecules, T$_1$, have been fully optimized by carrying out ab
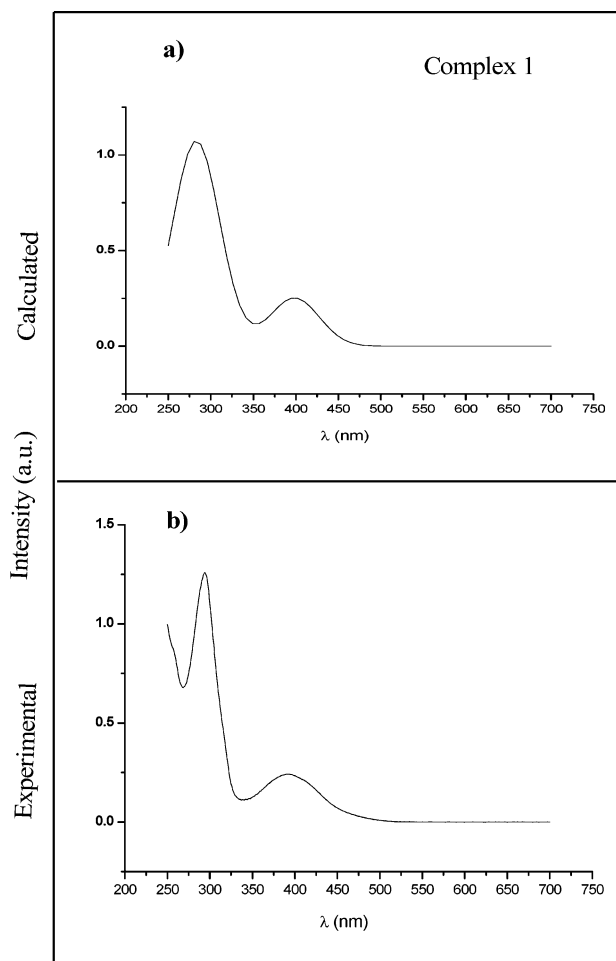
A Series of Halide Rhenium(I) Bipyridine Complexes

*J. Phys. Chem. A, Vol. 108, No. 32, 2004* **6805**



**Figure 6.** Comparison of calculated (a) and experimental (b) absorption spectra of the complex $ReCl(CO)_3(bpy)$. Experimental absorption data are measured in $CH_2Cl_2$ solution.



**Figure 7.** Comparison of calculated (a) and experimental (b) absorption spectra of the complex $ReCl(CO)_3(5,5'-2Br-bpy)$. Experimental absorption data are measured in $CH_2Cl_2$ solution.

initio CIS. The optimized structure parameters are shown as Table 8. The geometrical parameters for excited states have small differences from those of the ground state, and a general elongation of all the metal−ligand bond lengths is observed. For example, the Re−N bond distance in the triplet state is longer than that in the ground state by about $0.01-0.05$ Å, and the distance between the metal atom and carbon atom (Re−C) is also longer in the triplet state than in the ground state. As far as nonmetal bonds are concerned, some decrease and some increase.

We can predict the differences of the bond lengths between the ground ($S_0$) and triplet excited state ($T_1$) from nodal patterns.[42] Because the triplet state corresponds to an excitation from the HOMO to the LUMO in all considered complexes, we explore the bond-length variation by analyzing the HOMOs and LUMOs (see Figure 10). In the following section, we employed the complex $ReCl(CO)_3(4,4'-dibromo-bpy)$ as the example to analyze the bond lengths changes (see Table 6).

The LUMO has nodes across the N(1, 1′)−C(2, 2′), C(4, 4′)−C(5, 5′), C(2, 2′)−C(3, 3′), and C(5, 5′)−C(6, 6′) bonds, but the HOMO is bonding in these regions. Therefore one would expect elongation of these bonds; Table 9 shows that these bonds are in fact considerably longer in the excited state. The HOMO has a node across the C(3, 3′)−C(4, 4′) and C(2)−C(2′) bonds, while the LUMO is bonding. The data in Table 9 confirms the anticipated contraction of these bonds.

The spin density map for the lowest triplet states of complex **2**, reported in Figure 11, shows well the sharing of the two
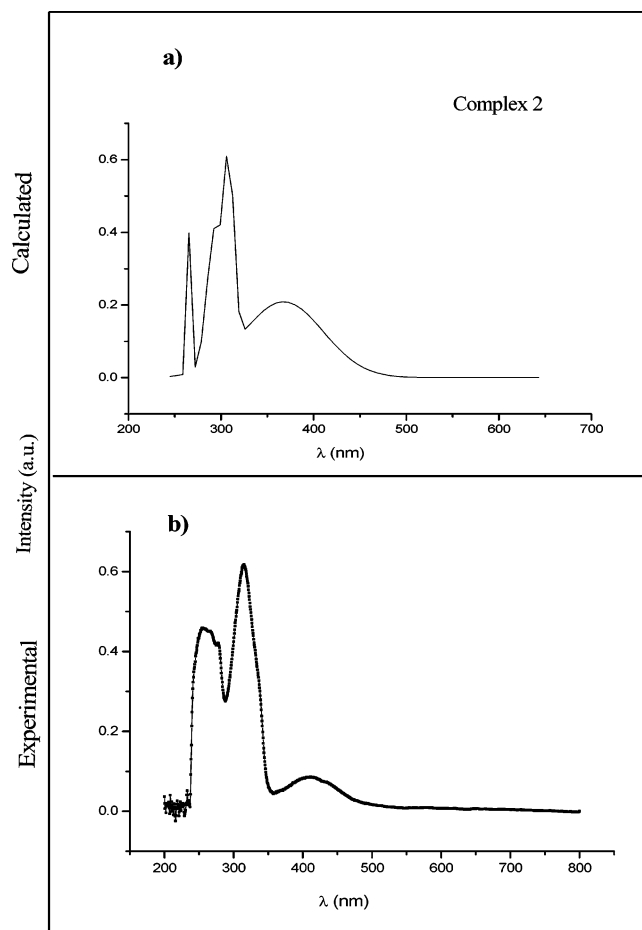
unpaired electrons among the metal (d orbital) and group Cl and the bipyridine ligand ($\pi^*$ orbital), with smaller contributions from the group CO. The four complexes have the similar behaviors. In general, all the geometry variations are consistent with the occupation of the $\pi^*$ orbitals of the bpy ligands depicted in Figure 10, and the variation path follows the bonding/antibonding scheme in such plots.

**Emissive Spectrum.** We employed the ab initio CIS method to optimize the lowest triplet state geometry, and at the excited triplet state geometry, TDDFT is used to calculate the emission spectra. The long-lived decay lifetime from experiment revealed that the photoluminescence for the four complexes is assigned as triplet-state charge transfer, and thus we only optimize the lowest triplet state ($T_1$) and calculate the triplet emission spectra. The results of the TDDFT calculations for complexes **1−4** are summarized in Table 10 and are compared with experimental emission data as depicted in Figure 12.

We list the lowest three triplet excited states and the photoluminescence for each complex corresponding to the lowest triplet $T_1$, which consists of the transition from HOMO to LUMO, and thus assigned as the mixed character between MLCT [d(Re) → $\pi^*$(bpy)] and LLCT [p(Cl) → $\pi^*$(bpy)]. Shih-Sheng Sun et al.[43] account the participation of these excited states largely for the decreasing emission quantum yields and shorter lifetimes of the emissive[3] MLCT excited states. Recent studies on rhenium(I) carbonyl systems have indicated that
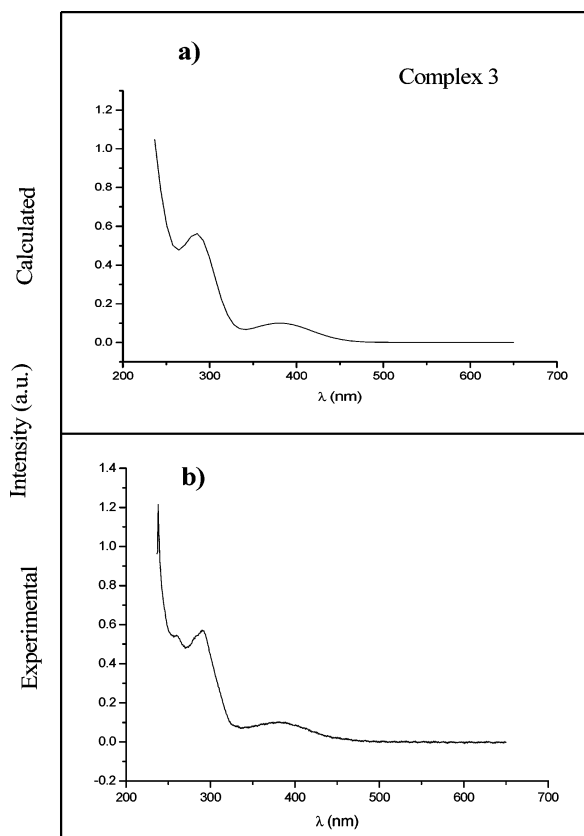
**6806** *J. Phys. Chem. A, Vol. 108, No. 32, 2004*

Yang et al.



**Figure 8.** Comparison of calculated (a) and experimental (b) absorption spectra of the complex $ReCl(CO)_3(4,4'-2CH_3-bpy)$. Experimental absorption data are measured in $CH_2Cl_2$ solution.
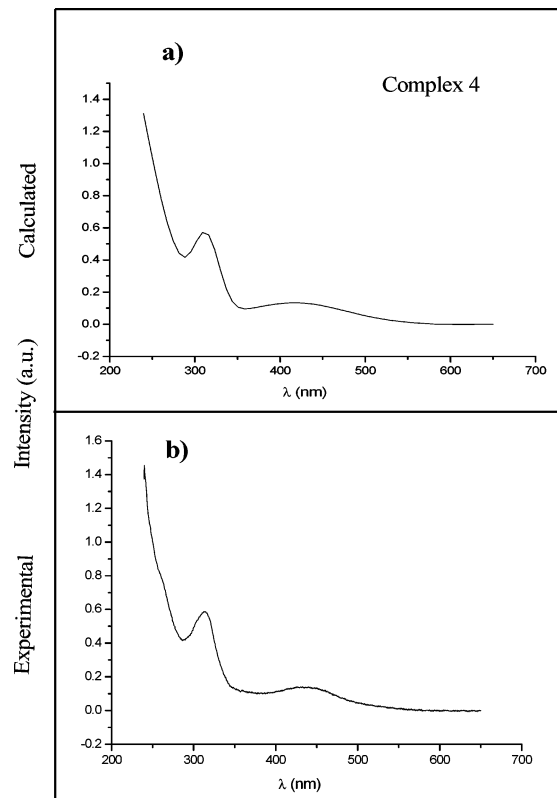


**Figure 9.** Comparison of calculated (a) and experimental (b) absorption spectra of the complex $ReCl(CO)_3(4,4'-2COOCH_3-bpy)$. Experimental absorption data are measured in $CH_2Cl_2$ solution.

emissive excited states of Re diimine complexes often have mixed MLCT and LLCT and, sometimes, IL characters. The
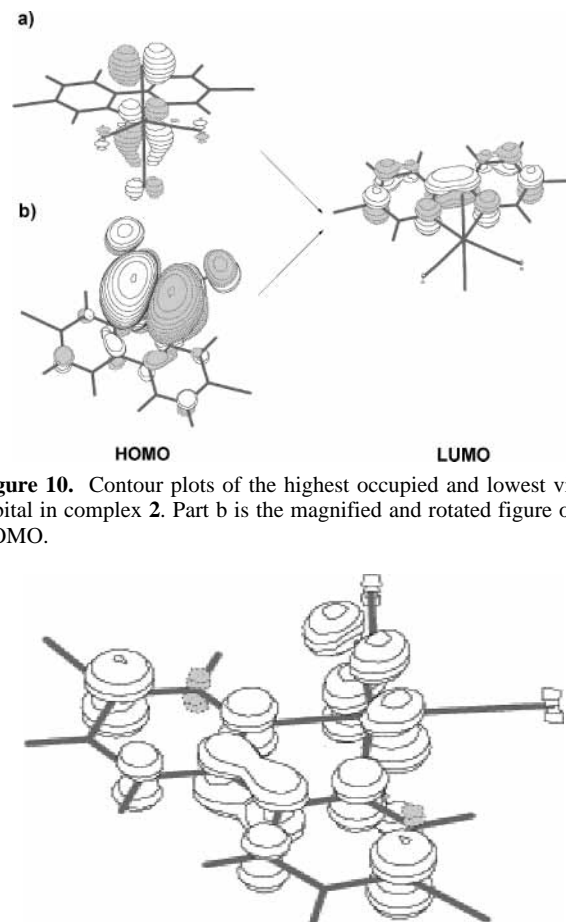


**Figure 10.** Contour plots of the highest occupied and lowest virtual orbital in complex **2**. Part b is the magnified and rotated figure of the HOMO.



**Figure 11.** Spin-density map for the lowest triplet state of $ReCl(CO)_3$-$(5,5'-2Br-bpy)$.

**TABLE 8: Main Geometrical Parameters (Å) of the Lowest Triplet State of the Four Complexes**

| bonds | **1** | **2** | **3** | **4** |
|---|---|---|---|---|
| $R[Re-N(1,1')]$ | 2.1789 | 2.1852 | 2.1852 | 2.1863 |
| $R[Re-C(1,1')]$ | 1.9596 | 1.9594 | 1.957 | 1.9598 |
| $R[Re-C(7)]$ | 1.9303 | 1.9298 | 1.9266 | 1.9301 |
| $R[Re-Cl]$ | 2.5612 | 2.5658 | 2.5728 | 2.5674 |

**TABLE 9: Calculated Bond Lengths of the Lowest Triplet State ($T_1$) and the Comparison to Corresponding Ground State Geometries ($S_0$) for Complex (2)**

| bond | $S_0$ | $T_1$ |
|---|---|---|
| $R[N(1,1')-C(2,2')]$ | 1.3733 | 1.4155 |
| $R[C(4,4')-C(5,5')]$ | 1.4009 | 1.4332 |
| $R[C(3,3')-C(4,4')]$ | 1.4005 | 1.367 |
| $R[C(2,2')-C(3,3')]$ | 1.4075 | 1.4545 |
| $R[C(5,5')-C(6,6')]$ | 1.4049 | 1.4058 |
| $R[C(2)-C(2')]$ | 1.473 | 1.4082 |

detailed excited-state character influences relaxation pathways and rates.[44]

Apart for transition character discussed above, our calculations also reproduce (even if not quantitatively) the red or blue shift, which affected by substituents changes observed in going from the four complexes having identical chemical environments. Consistent with experimental data, analysis for molecular orbitals and absorption spectra, an electron-releasing group leads to a blue shift and an electron-withdrawing group leads to red shift. The calculated emission peak at 757 nm (1.64 eV) for complex **3** is blue shifted, and the peaks at 797 (1.56) and at
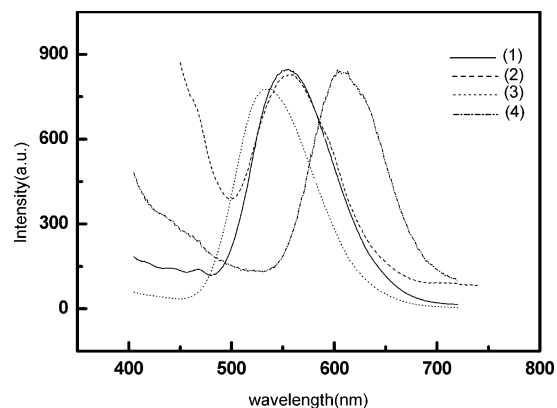
A Series of Halide Rhenium(I) Bipyridine Complexes

*J. Phys. Chem. A, Vol. 108, No. 32, 2004* **6807**



**Figure 12.** Experimental photoluminescence spectra of complexes 1−4 measured in polycarbonate film.

**TABLE 10: Computed TDDFT Excitation Energies (nm) for the Lowest Triplet States of All the Considered Complexes with Experimental Data**

| | excitation | $E_{cal}$, eV | $\lambda_{cal}$, nm | $E_{exp}$, eV | $\lambda_{exp}$, nm | character |
|---|---|---|---|---|---|---|
| | | | $ReCl(CO)_3(bpy)$ | | | |
| $T_1(A'')$ | 73 → 74 | 1.66 | 743 | 2.24 | 555 540[36] | MLCT/LLCT |
| $T_2(A')$ | 72 → 74 | 1.71 | 726 | | | |
| $T_3(A')$ | 71 → 74 | 2.23 | 557 | | | |
| | | | $ReCl(CO)_3(5,5'$-dibromo-bpy) | | | |
| $T_1(A'')$ | 79 → 80 | 1.56 | 797 | 2.23 | 556 | MLCT/LLCT |
| $T_2(A')$ | 78 → 80 | 1.69 | 734 | | | |
| $T_3(A')$ | 77 → 80 | 2.25 | 552 | | | |
| | | | $ReCl(CO)_3(4,4'$-dimethyl-bpy) | | | |
| $T_1(A'')$ | 81 → 82 | 1.64 | 757 | 2.33 | 533 530[36] | MLCT/LLCT |
| $T_2(A')$ | 80 → 82 | 1.70 | 729 | | | |
| $T_3(A')$ | 79 → 82 | 2.33 | 531 | | | |
| | | | $ReCl(CO)_3(4,4'$-dimethylformyl-bpy) | | | |
| $T_1(A'')$ | 103 → 104 | 1.51 | 832 | 2.05 | 605 | MLCT/LLCT |
| $T_2(A')$ | 102 → 104 | 1.61 | 768 | | | |
| $T_3(A')$ | 101 → 104 | 2.15 | 576 | | | |

832 nm (1.51 eV) for complexes **2** and **4**, respectively, are red shifted compared with complex **1**, the peak at 743 nm (1.66 eV).

From Table 10, there exist some deviations between calculated and experimental data for emission spectra. Concerning the reasons of producing such deviations, we want to stress several points. First is the solvent effect. Usually the studied system is put in a gas phase environment for a quantum method, whereas its laid in a solution environment in experiment, and our limited studies did not take the solvent effects into account and thus not add effects rectification. Second is the limit of the quantum chemical approach. CIS was employed to optimize the lowest triplet excited state, and despite the name, CIS represents for excited states a general zeroth-order method and does not include double and third excitations, whereas it is necessary for discussing electron correlation. Other DFT calculations overestimate halide contributions in metal−halide complexes, especially if a low-valent metal atom is involved.[34] In addition, the more detailed interpretation of phosphorescence properties will await the inclusion of spin−orbit coupling effects that are not included in these TDDFT results. We hope to investigate these effects in future studies.

## Conclusions

In this paper, we have applied DFT methods to analyze ground- and excited-state properties of the complex **1** and the

related complexes ′**2**, ′**3**, and ′**4**. The ground-state structures are calculated by B3LYP density functional and are in good agreement with available crystallographic studies. Most of the highest-occupied orbitals are Re (5d) in character, with an almost equal admixture of Cl group with exception for $HOMO_{-2}$, which is dominated by Re (5d). The spin densities in the cations show over 0.50 electrons on the metal center and over 0.30 electrons on the group Cl for each molecule, which is basically consistent with this analysis. The lowest virtual orbitals are totally $\pi^*$ (bpy) in character, as also reflected in the spin densities in the anion.

Forty singlet and thirty-five triplet excited states are examined using TDDFT. The low-energy absorption, which the light-emitting is concerned about, is all assigned as the mixture of MLCT [d(Re) → $\pi^*$(bpy)] and LLCT [p(Cl) → $\pi^*$(bpy)]. Looking at Table 3, a good agreement between the computed absorption bands and the reported experimental bands in the ref 35 can be found. The lowest triplet excited-state structures of the four molecules are obtained using CIS method. The emission band has been supposed to be an electronic transition between the ground and the triplet excited state $T_1$ with the character of the mixture of MLCT and LLCT for all considered complexes.

The results of absorption and emission spectral fitting give insight into the effect that changes in X have on the structure of the bpy acceptor ligand. As might have been expected, the effect is less profound at the d orbitals than at the $\pi^*$ orbitals since the substituent changes are made at the ligand. The electron-releasing group −$CH_3$ leads to both absorption and emission spectra blue shifts due to the increased energy of LUMO which results in the increased HOMO−LUMO band gap, and electron-withdrawing groups −Br and −$COOCH_3$ lead to red shift due to the decreased energies of LUMOs which decrease the energy band gaps. Furthermore, we find large Stoke shifts for the four complexes. The results indicate that application of TDDFT calculations is reliable for studying the system containing transition metals, but at the same time, it has some drawbacks, such as overestimating the compositions of halides in low-valent metal complexes and without considers spin−orbit coupling effects.

## References and Notes

(1) Kingsborough, R. P.; Swager, T. M. *Prog. Inorg. Chem.* **1999**, *48*, 123.

(2) Wang, Q.; Wang, L.; Yu, L. *J. Am. Chem. Soc.* **1998**, *130*, 12860.

(3) Wang, B.; Wasielewski, M. R. *J. Am. Chem. Soc.* **1997**, *119*, 12.

(4) Walters, K. A.; Troouillet, L.; Guillerez, S.; Schanze, K. S. *Inorg. Chem.* **2000**, *39*, 5496.

(5) Ley, K. D.; Whittle, C. E.; Bartverger, M. D.; Schanze, K. S. *J. Am. Chem. Soc.* **1997**, *119*, 3423−3424

(6) Ley, K. D.; Li, Y. T.; Johnson, J. V.; Powell, D. H.; K. S. *Chem. Commun.* **1999**, 1749−1750.

(7) Walters, K. A.; Ley, K. D.; Cavalaheiro, C. S. P.; Miller, S. E.; Gosztola, D.; Wasielewski, M. R.; Bussandri, A. P.; van Willigen, H.; Schanze, K. S. *J. Am. Chem. Soc.* **2001**, *123*, 8329−8342.

(8) Li, Y.; Whittle, C. E.; Walters, K. A.; Ley, K. D.; Schanze, K. S. *MRS Symp. Proc.*, in press.

(9) Cahen, D.; Grätzel, M.; Guillemoles, J. F.; Hodes, G. In *Electrochemistry of nanomaterials*; Hodes, G., Ed.; Wiley-VCH: Weiheim, Germany, 2001.

(10) Juris, A.; Barigelletti, F.; Campagna, S.; Balzain, V.; Belser, p.; von Zelewski, A. *Coord. Chem. Rev.* **1988**, *84*, 85.

(11) Han, Y.-K.; Lee, S. U. **2002**, *366*, 9−16.

(12) Lo, K. K.-W.; Hui, W.-K.; Ng, D. C.-M.; Cheung, K.-K. *Inorg. Chem.* **2002**, *41*, 40−46.

(13) Walters, K. A.; Premvardhan, L. L.; Liu, Y.; Peteanu, L. A.; Schanze, K. S. *Chem. Phys. Lett.* **2001**, *339*, 255−262.

(14) Wolfbauer, G.; Bond, A. M.; Deacon, G. B.; MacFarlane, D. R.; Spiccia L. *J. Am. Chem. Soc.* **2000**, *122*, 130−142.

(15) Rensmo, H.; Lunell, S.; Siegbahn, H. *J. Photochem. Photobiol.* A **1998**, *114*, 117.

(16) Albano, G.; Belser, P.; Daul, C. *Inorg. Chem.* **2001**, *40*, 1408.

(17) Nazeeruddin, Md. K.; Zakeeruddin, S. M.; Humphry-Baker, R.; Gorelsky, S. I.; Lever, A. B. P.; Gratzel, M. *Coord. Chem. Rev.* **2000**, *208*, 213.

(18) Guillemoles, J.-F.; Barone, V.; Joubert, L.; Adamo, C. *J. Phys. Chem. A* **2002**, *106*, 11354−11360

(19) Shinozaki, K.; Takahashi, N. *Inorg. Chem.* **1996**, *35*, 3917.

(20) Koch, W.; Holthausen, M. C. *A Chemist's Guide to Density Functional Theory*; Wiley-VCH: Weinheim, Germany, 2000.

(21) Adamo, C.; di Matteo, Barone, V. *Adv. Quantum Chem.* **1999**, *36*, 4.

(22) Runge, E.; Gross, E. K. *U. Phys. Rev. Lett.* **1996**, *76*, 1212.

(23) Bauernschmitt, R.; Ahlrichs, R. *Chem. Phys. Lett.* **1996**, *256*, 454.

(24) Casida, M. K.; Jamorski, C.; Casida, K. C.; Salahub, D. R. *J. Chem. Phys.* **1998**, *108*, 4439.

(25) Stratmann, R. E.; Scuseria, G. E.; Frisch, M. *J. Chem. Phys.* **1998**, *109*, 8128.

(26) Lee, C.; Yang, W.; Parr, R. G. *Phys. Rev.* B **1998**, *37*, 785.

(27) Becke, A. D. *J. Chem. Phys.* **1993**, *98*, 5648.

(28) Rosa, A.; Baerends, E. J.; van Gisbergen, S. J. A.; van Lenthe, E.; Gooeneveld, J. A.; Snihders, J. G. *J. Am. Chem. Soc.* **1999**, *121*, 10356.

(29) Adamo, C.; Bareone, V. *Theo. Chem. Acc.* **2000**, *105*, 169−172.

(30) Boulet, P.; Chermett, H.; Daul, C.; Gilardoni, F.; Rogemond, F.; Weber, J.; Zuber, G. J. *Phys. Chem. A* **2001**, *105*, 885−894.

(31) Farrell, I. R.; van Slageren, J.; Zalis, S.; Vlcek, A. *Inorg. Chim. Acta* **2001**, *315*, 44−52.

(32) Foresman, J. B.; Head-Gordon, M.; Pople, J. A. Frisch, M. J. *J. Phys. Chem.* **1996**, *100*, 9047.

(33) Dong, Y.-B.; Yang, L.; Cheung, K.-K.; Mayr, A. *J. Organomet. Chem.* **2000**, *598*, 55−62.

(34) Turki, M.; Daniel, C.; Záli×f0, S. *J. Am. Chem. Soc.* **2001**, *123*, 11431−11440.

(35) Stufkens, D. J.; Vlĉek, A., Jr. *Coord. Chem. Rev.* **1998**, *177*, 127.

(36) Nieawenhuis, H. A.; Stufkens, Derk, J. *J. Am. Chem. Soc.* **1995**, *117*, 5579−5585.

(37) Luong, J. C.; Nadjo, L.; Wrighton, M. S. *J. Am. Chem. Soc.* **1978**, *100*, 5790.

(38) Burrow, P. E.; Shen, Z. *J. Appl. Phys.* **1996**, *79*, 7991−8006.

(39) Curioni, A.; Andreoni, W. *IBM J. Res. Dev.* **2001**, *45*, 101−113.

(40) Hay, J. P. *J. Phys. Chem.* A **2002**, *106*, 1634.

(41) Worl, L. A.; Duesing, R.; Chen, P.; Della Ciana, Meyer, T. J. *J. Chem. Soc. Dalton Trans.* **1991**, 849.

(42) Mathew, D.; Halls; H. Bernhard Schlegel. *Chem. Mater.* **2001**, *13*, 2632−2640.

(43) Sun, S.-S.; Tran, D. T.; Odongo, O. S.; Lees, A. J. *Inorg. Chem.* **2002**, *41*, 132−135.

(44) (a) Ferraudi, G.; Feliz, M.; Wolcan, E.; Hsu, I.; Moya, S. A.; Guerrero. J. *J. Phys. Chem.* **1995**, *99*, 4929. (b) Guerrero, J.; Piro, O. E.; Feliz, M. R.; Ferraudi, G.; Moya, S. A. *Organometallics* **2001**, *20*, 2842.